energy&fuels

pubs.acs.org/EF

Article

Viscosity and Density of Narrow Distillation Cuts from Refined Petroleum- and Synthetic-Derived Distillates in the −60 to +60 °C Range

Felix Link* and Arno de Klerk

Cite This: *Energy Fuels* 2022, 36, 12563−12579

Read Online

ACCESS | Metrics & More | Article Recommendations | Supporting Information

ABSTRACT: Aviation turbine fuel (jet fuel) must remain fluid enough for use at low temperatures typically experienced during high-altitude flights. The viscosity−temperature relationship of petroleum-derived jet fuel is described by the MacCoull correlation in ASTM D341. The maximum kinematic viscosity of jet fuel at −20 °C is regulated by specification, but for long-distance flights, viscosity of <12 mm^2 s^{-1} at −40 °C is important. For synthesized paraffinic kerosene (SPK) to be approved as a synthetic jet fuel, compliance with these viscosity limits is imperative. A petroleum-based kerosene and SPK from wax hydrocracking were distilled into narrow cut (5 °C range) fractions, and for each narrow cut, density, viscosity, and refractive index values were measured over the temperature range from +60 to −60 °C. The viscosity−temperature dependences of the petroleum-derived and synthetic narrow cuts were described with comparable accuracy (relative deviation <5%) by the MacCoull correlation. Calculation of kinematic viscosity at −40 °C by extrapolating data measured at ≥−20 °C underpredicted viscosity for >200 °C boiling kerosene cuts, with a maximum relative deviation of 6.6%. The freezing point is another jet fuel property that is regulated by specification. Good agreement (±1.3 °C) was found between the end of the melting endotherm obtained by differential scanning calorimetry (DSC) and the freezing point determined according to ASTM D2386. Local maxima/minima in the freezing point of distillation cuts with increasing boiling point were observed and could be related to the freezing point characteristics of the *n*-alkanes.

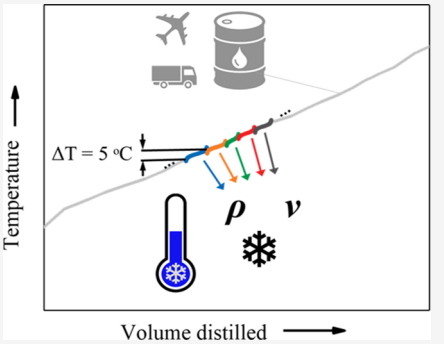

1. INTRODUCTION

The aviation turbine fuel (jet fuel) in aircraft operating at high altitudes decreases in temperature over time as the wing tanks are exposed to outside temperatures of around −60 °C.[1] Aircraft operating from airports at high latitudes may even be exposed to low outside temperatures in winter on the ground during refueling prior to takeoff, exacerbating fuel cooling. Flow assurance of fuel during flight is imperative. For this reason, the maximum freezing point specification of Jet A-1 is −47 °C.[2] A special grade, Jet B, with maximum freezing point specification of −50 °C is used for extreme cold service.[3]

The viscosity of Jet A-1 is also regulated, with a maximum of 8.0 mm^2 s^{-1} at −20 °C.[2] The purpose of the low-temperature viscosity specification in jet fuel is to ensure fuel pumpability at low temperatures, but foremost, it is to ensure proper operation of the auxiliary power unit in the aircraft. This unit must be able to start under any ground or flight conditions, and the fuel in the fuel line to this unit may approach −40 °C after a long flight. The droplet size distribution and spray pattern in the auxiliary power unit is sensitive to the viscosity, which degrades visibly at a kinematic viscosity higher than 12 mm^2 s^{-1} at −40 °C.[1]

At present, jet fuel viscosity at −40 °C is only regulated for some semi-synthetic jet fuels, including those containing synthesized paraffinic kerosene (SPK) derived from hydro-processed esters and fatty acids (HEFA-SPK). It is not regulated for petroleum-derived jet fuel and semi-synthetic jet fuels containing synthesized paraffinic kerosene derived from Fischer−Tropsch synthesis (FT-SPK), or the same containing aromatics (FT-SPK/A).[4] For those fuels, the −40 °C viscosity threshold for reliable operation of the auxiliary power unit relies on the assumption that the low-temperature viscosity can be accurately predicted by extrapolation using MacCoull's viscosity−temperature equation recommended in ASTM D341.[5] For ease of reference, MacCoull's equation is repeated here as eq 1.

$$\log\log(\upsilon + 0.7 + \exp(-1.47 - 1.84\upsilon - 0.51\upsilon^2)) = A - B\cdot\log(T) \quad (1)$$

where T is temperature (K) and υ is the kinematic viscosity at temperature T (mm^2 s^{-1}).

Received: August 5, 2022
Revised: September 16, 2022
Published: October 10, 2022

https://doi.org/10.1021/acs.energyfuels.2c02625
Energy Fuels 2022, 36, 12563−12579

It is worthwhile pointing out that the temperature dependence of viscosity of Jet A-1 (JP-8) and Jet B (JP-4) is slightly different.[3] In addition to this, there is variation in the actual properties of on-specification Jet A-1 fuels.[6] Within the diversity of petroleum-derived jet fuels, the Boeing Fuel Laboratory already pointed out examples of Jet A-1 that met the −20 °C viscosity specification but that had a viscosity of >12 $mm^2 s^{-1}$ at −40 °C.[6] There are therefore examples of petroleum-derived jet fuel where the change in viscosity at cold temperatures deviated from the predicted relationship.

In the development of synthetic jet fuels, which are not petroleum-derived, it was shown that for FT-SPK, the viscosity−temperature relationship was equally described by eq 1.[7] At the same time, it is recognized that the value for the viscosity−temperature slope, the regression constant *B* in eq 1, may not have the same temperature dependence as that of petroleum-derived jet fuels. The viscosity at −40 °C is therefore one of the properties required for the prescreening of synthetic jet fuel candidates.[4,8,9] A limited number of investigations dealing with synthetic jet fuel properties reported sufficient data to calculate the temperature dependence of viscosity[7,10−12] but few experimentally measured viscosity values at <−20 °C.

The primary purpose of this investigation was to determine the temperature-dependent viscosity of narrow distillation cuts of distillates that could be used to formulate a conventional Jet A (or A-1) and a synthetic paraffinic kerosene blendstock for creating an alternative Jet A (or A-1) finished fuel as described in ASTM D7566 Annex 1.[4] To do so, a wax hydrocracking product that is a proxy for an FT-SPK was fractionated in narrow boiling cuts (5 °C boiling range), which included material in the kerosene and the atmospheric gas oil range. Each boiling cut was characterized in terms of temperature-dependent viscosity, density, and refractive index. Specifically, the viscosity and density were measured over the −60 to+60 °C range. Additionally, the relationship between the onset of freezing and the end of the melting endotherm determined by differential scanning calorimetry (DSC), as well as the optically determined freezing point, was investigated. For control purposes, the same analyses were performed on petroleum-derived kerosene.

2. EXPERIMENTAL SECTION

2.1. Materials. Two materials were distilled for the determination of the low-temperature properties of narrow distillation cuts, one petroleum-based and one synthetic.

The petroleum-based material is a hydrotreated heavy naphtha and kerosene cut with a boiling range of 110−270 °C (simulated distillation, ASTM D7169[13]) with an aromatic fraction of 19 wt %. It was obtained from Husky Energy. Additional compositional information and a gas chromatogram of the material are shown in Figure S1 and Table S1 in the Supporting Information.

The synthetic distillate was the product of hydrocracking of a paraffinic wax over a $Pt/SiO_2−Al_2O_3$ catalyst at 2 MPa.[14] The composition of the parent paraffin wax is shown in Table S2 in the Supporting Information. Most of the hydrocracked material comprises linear and branched alkanes, but on account of the low operating pressure, the hydrocracked product also contained some aromatics and cycloalkanes. Chromatographic analysis of single cuts of the distillate in the boiling range below 200 °C indicated an aromatic content of 1−3 wt % and a cycloalkane content of 5−10 wt %.[14] Compositional information and boiling point distribution of the parent wax and hydrocracking product are available in ref 14.

2.2. Equipment and Procedure. For the preparation of distillation cuts, a B/R instrument 18 CODS distillation system was used. Distillation was carried out in batches of about 700 mL each, with a reflux ratio of 20 at atmospheric pressure (around 93 kPa in Edmonton, AB) up to a boiling point of 200 °C. The remaining heavier material was distilled at an absolute pressure of 14 kPa with the same reflux ratio.

For both materials, the distillation fraction boiling below 140 °C, the naphtha fraction, was collected for material balance, but not considered for analysis. Material boiling above 140 °C was separated into narrow distillation cuts with a boiling point difference of 5 °C. For the petroleum-based kerosene, materials with a boiling point above 255 °C were discarded from analysis because the amount of material remaining in the still was insufficient for further separation. The final cut collected for the synthetic distillate had a boiling range of 320−325 °C.

The mass recovered in each distillation cut during the distillation of the petroleum-based kerosene is reported, along with compositional information, in the Supporting Information (Table S3). Similar data for the preparation of the synthetic distillate cuts has been reported before[14] and is repeated in the Supporting Information (Table S4). Both materials were distilled without discontinuities in the distillation profile. The distillation cuts were stored in closed vials in a refrigerator at −18 °C. Transfer of samples from vials to analysis equipment was carried out rapidly to prevent volatilization. Cuts with boiling point >260 °C were kept at room temperature until any crystals of frozen material were dissolved before analysis.

2.3. Analyses. *2.3.1. Refractive Index.* Refractive index measurements were performed relative to air using the sodium D-line (589 nm) with an Anton Paar Abbemat 200 refractometer. The refractive index was determined at four temperatures, 20, 25, 40, and 60 °C, for all distillation cuts.

2.3.2. Differential Scanning Calorimetry. The thermal behavior of the distillation cuts at low temperatures was investigated via differential scanning calorimetry (DSC). Between 8 and 20 mg of sample was weighed into 40 μL aluminum crucibles with perforated lids on an analytical balance (Mettler Toledo, model XS105). The crucibles were transferred to an atmospheric pressure differential scanning calorimeter (Mettler Toledo DSC 1). This equipment is a heat flow (disk)-type calorimeter equipped with an FRS-5 sensor. An empty 40 μL aluminum crucible with a perforated lid was used as the reference. The cell was flushed, and a nitrogen atmosphere was maintained by a constant flow of 40 mL min^{-1} nitrogen. The heat flow was measured during cooling of the samples from 25 °C at a rate of −2 °C min^{-1} to −70 °C, a hold time of 5 min at −70 °C, and subsequent heat-up to 0 °C at a rate of 2 °C min^{-1}. All analyses were corrected by subtraction of the signal determined from a blank experiment (empty crucible).

To ensure proper operation, DSC analysis was carried out using the above-mentioned method with *n*-nonane (>99%, Acros Organics) and *n*-decane (99%, Alfa Aesar) before and after the analysis of the distillation cuts. The end of the melting endotherm correlated within a range of ±0.5 °C with the literature-reported melting points of −54 and −30 °C for *n*-nonane and *n*-decane, respectively.[15] Then enthalpy of fusion was determined from integration of the heat flow signal below the freezing and melting peaks in the calorigram. The enthalpy of fusion (average of freezing and melting) was determined to be 191 J g^{-1} for *n*-decane. The difference between the calculated enthalpy during melting and freezing was lower than the difference of the average values to literature-reported enthalpies, which was 5% relative.[16]

2.3.3. Determination of Viscosity and Density. Density and viscosity were measured in an Anton Paar SVM 3001 Cold Properties viscosimeter. The density was measured via a U-tube oscillator within the instrument according to ASTM D4052.[17] The viscosity was measured in a Stabinger viscosimeter-type cell (ASTM D7042[18]). The temperature of the U-tube oscillator and the viscosity cell was maintained via a Peltier element counter-cooled by a chiller. Density and viscosity can be measured down to a minimum temperature of −60 °C.

About 3 mL of sample was filled into the instrument after cleaning it with toluene and drying with dry compressed air. The dynamic viscosity and density were determined by starting at 60 °C. Viscosity and density analyses were conducted after temperature stability within 0.005 °C for 90 s. Steady-state viscosity was recorded after viscosity measurements were constant within a relative range of 0.07% for 60 s, and steady-state density was recorded after the density measurements were constant

https://doi.org/10.1021/acs.energyfuels.2c02625
Energy Fuels 2022, 36, 12563−12579

within 0.0001 g cm^{-1} for 60 s. These constraints were added to ensure that sample volatilization did not interfere with the results. The sample was then cooled to the next determination temperature of 40 °C, where density and viscosity were analogously determined. From 40 to 0 °C, the density and viscosity were recorded in 10 °C steps with an additional analysis at 15 °C. Analyses below 0 °C were carried out in 5 °C steps until the onset of freezing or −60 °C if freezing did not occur.

The instrument was calibrated by the manufacturer prior to the analyses of the distillation cuts. After the analysis of the cuts, the viscosity and density of two standards, a JF-1L low-temperature viscosity standard (Paragon Scientific) and an S3 general viscosity standard (Paragon Scientific), were determined. The relative deviation from the nominal viscosity and density of the standards was below 1%.

2.3.4. Optical Determination of Freezing Point. The freezing point was determined in the same instrument as viscosity and density (Anton Paar SVM 3001 Cold Properties) but using a different measuring mode. When a sample is introduced to the instrument, it fills a transparent optical cell along with the density and viscosity cell. The intensity of monochromatic parallel rays of light that pass through the cell is measured, and the transmittance of transparent liquid samples is set to 100%. The sample is cooled until crystallization of sample molecules leads to a drop in transmittance close to 0%. The temperature is maintained for 5 min to achieve thermal and phase equilibration of the sample. During subsequent heat-up, the instrument determines the temperature at which 60% transmittance is restored. The freezing point is then calculated by adding an offset of 4 °C to the temperature at 60% transmittance. This offset was calibrated by the instrument manufacturer to match the freezing point of reference samples with known freezing points determined by ASTM D2386.[19]

2.3.5. High-Performance Liquid Chromatography (HPLC) for Determination of Aromatics. The volume fraction of mono- and diaromatic hydrocarbons was determined for the petroleum-based kerosene cuts via HPLC using a Waters Alliance e2695 instrument. The separation was carried out using a Waters Spherisorb NH_2 column (4.6 mm × 300 mm, 3 μm particle size) with *n*-heptane (HPLC grade, Fisher) as the mobile phase. Calibration and analyses were carried out following ASTM D6379.[20]

3. RESULTS

3.1. Refractive Index and Aromatic Content. The refractive indices determined at 20, 25, 40, and 60 °C of all distillation cuts of the petroleum-based kerosene and synthetic distillate are summarized in Tables S5 and S6, respectively.

All samples show a decreasing linear correlation between the refractive index and the temperature of measurement, as indicated by the slope of the refractive index with respect to temperature, dn/dT. The correlation coefficient (r^2) of linear regression of the refractive index with respect to temperature was 0.999 or better for all measurements, providing an internal consistency check on the measured data. The aromatic content in the cuts of the petroleum-based kerosene was determined by HPLC. The aromatic volume fractions are shown in Figure S2 in the Supporting Information. The aromatic content in the synthetic distillate was low.[14]

3.2. Density and Viscosity. Density and viscosity data were recorded for all distillation cuts at various temperatures. The results from density analysis for petroleum-based kerosene and synthetic distillate cuts are summarized in Tables 1 and 2, respectively. The observed increase in density with increasing boiling point of cuts from both synthetic and petroleum-based materials is expected, and it is in line with other studies analyzing cuts of hydrocarbon materials.[21−23]

Over the temperature range measured, the relationship between liquid density and temperature was linear, with a correlation coefficient (r^2) of 0.998 or better. The slope of the liquid density index with respect to temperature, $d\rho/dT$, for the same distillation cut of the petroleum-based and synthetic material was within 2% relative to each other. For the petroleum-based kerosene, the values for $d\rho/dT$ increased from −0.78 to −0.70 kg m^{-3} K^{-1} for the cuts in the range of 140−255 °C. For the synthetic distillate, the values for $d\rho/dT$ increased from −0.77 to −0.66 kg m^{-3} K^{-1} for the cuts in the range of 140−325 °C.

The dynamic viscosities at all analyzed temperatures are shown in Table 3 for petroleum-based kerosene cuts and in Table 4 for synthetic distillate cuts. Calculated kinematic viscosities, shear rate, and shear stress for all distillation cuts are shown in Tables S7 and S8 in the Supporting Information.

3.3. Solid−Liquid Phase Change Behavior. The solid−liquid phase change behavior of each of the individual distillation cuts was determined by DSC, as illustrated by a representative calorigram shown in Figure 1.

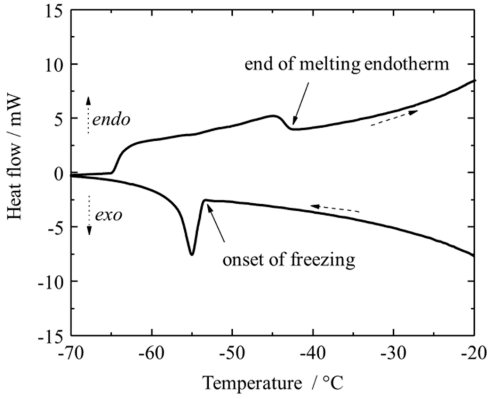

Figure 1. Illustrative calorigram showing the onset of freezing and the end of the melting endotherm of a narrow distillation cut. Shown here is the relevant part of the calorigram of the synthetic kerosene cut with a boiling point of 230−235 °C.

Upon cool-down, the heat flux slowly increases, caused by changes in heat capacity of the sample.[24] The heat capacity was not determined as part of this study. The freezing process can be clearly identified by a peak representing the heat release during crystallization. The beginning of the slope of this peak is marked as the onset of freezing in Figure 1. After further cooling and holding the temperature at −70 °C, melting of the sample is indicated by a broader melting endotherm during heat-up. The end of the melting endotherm represents the temperature at which the final hydrocarbon crystals have dissolved in the previously melted liquid part of the sample, and it is indicated in Figure 1.

Both the onset of freezing and the end of the melting endotherm were determined for all distillation cuts for which freezing could be induced at −70 °C. They are summarized together with the optically determined freezing points for the petroleum-based kerosene and the synthetic distillate cuts in Tables 5 and 6, respectively.

Additionally, the enthalpy of phase change during freezing and the enthalpy of phase change during melting were calculated by fitting a spline as the baseline and integrating the area of the freezing and melting events. These values are reported in Tables 5 and 6. From triplicate analyses of the synthetic distillate cut with a boiling range of 230−235 °C, the uncertainty of determination for the enthalpy of phase change during freezing and melting (repeatability) is estimated to be ±2 J g^{-1}.

https://doi.org/10.1021/acs.energyfuels.2c02625
Energy Fuels 2022, 36, 12563−12579

Table 1. Density of Petroleum-Based Kerosene Cuts at All Measured Temperatures[a]

	density at indicated measurement temperatures in °C (kg m^{-3})																			
initial boiling point (°C)	60	40	30	25	20	15	10	0	−5	−10	−15	−20	−25	−30	−35	−40	−45	−50	−55	−60
140	[b]	748.5	757.1	760.9	764.6	768.7	772.6	780.2	784.2	788.0	791.9	795.8	799.6	803.5	807.4	811.2	815.1	819.1	823.0	826.8
145	[b]	756.0	764.2	768.1	772.1	776.0	779.9	787.8	791.6	795.5	799.3	803.2	807.1	811.0	814.9	818.8	822.7	826.6	830.4	834.3
150	[b]	759.9	768.2	772.1	776.0	779.9	783.8	791.6	795.5	799.3	803.2	807.0	810.8	814.7	818.6	822.5	826.3	830.2	834.0	837.9
155	[b]	766.2	774.5	778.3	782.1	786.0	789.9	797.7	801.5	805.3	809.1	812.9	816.7	820.5	824.4	828.2	832.1	835.9	839.8	843.6
160	[b]	771.4	779.5	783.3	787.2	791.0	794.9	802.5	806.4	810.2	814.0	817.8	821.6	825.4	829.3	833.1	836.9	840.8	844.6	848.4
165	[b]	775.3	783.5	787.3	791.1	795.0	798.8	806.5	810.3	814.1	817.9	821.7	825.5	829.3	833.1	836.9	840.7	844.6	848.4	852.2
170	[b]	778.3	786.4	790.2	794.0	797.9	801.7	809.4	813.1	816.9	820.7	824.4	828.2	831.9	835.7	839.4	843.0	847.0	850.8	854.6
175	[b]	780.5	788.6	792.3	796.0	799.8	803.6	811.2	814.9	818.7	822.4	826.1	829.8	833.6	837.4	841.2	844.9	848.7	852.5	856.2
180	769.0	784.8	792.4	796.0	799.8	803.5	807.3	814.8	818.5	822.3	826.0	829.7	833.4	837.2	840.9	844.7	848.5	852.2	856.0	859.7
185	772.8	788.6	796.2	799.9	803.6	807.4	811.1	818.6	822.3	826.0	829.7	833.4	837.1	840.8	844.5	848.3	852.0	855.8	859.5	863.3
190	777.8	793.2	800.8	804.4	808.1	811.8	815.5	823.0	826.7	830.3	834.0	837.7	841.1	844.9	848.6	852.4	856.0	859.8	863.5	[c]
195	781.6	797.0	804.6	808.1	811.8	815.5	819.2	826.6	830.3	834.0	837.6	841.3	844.9	848.6	852.3	856.1	859.8	863.5	867.2	[c]
200	785.9	801.0	808.7	812.2	815.9	819.6	823.3	830.7	834.3	838.0	841.6	845.2	848.9	852.5	856.2	859.9	863.6	867.3	871.0	[c]
205	791.1	806.3	814.0	817.5	821.2	824.9	828.5	835.9	839.5	843.2	846.8	850.4	854.1	857.7	861.4	865.1	868.8	872.5	876.2	[c]
210	793.2	808.2	815.8	819.3	823.0	826.6	830.3	837.6	841.2	844.9	848.5	852.1	855.5	859.3	863.0	866.7	870.3	874.0	877.6	[c]
215	792.8	807.7	815.2	818.6	822.3	825.8	829.2	836.3	839.9	843.4	846.9	850.5	854.1	857.7	861.4	865.1	868.8	872.5	[c]	[c]
220	794.0	808.9	816.5	819.9	823.6	827.2	830.8	838.1	841.6	845.2	848.8	852.4	855.9	859.6	863.2	866.8	870.5	874.1	[c]	[c]
225	797.0	811.9	819.4	822.9	826.5	830.1	833.7	840.9	844.4	848.1	851.7	855.2	858.8	862.4	866.0	869.6	873.2	[c]	[c]	[c]
230	799.8	814.4	821.5	825.3	829.0	832.5	836.1	843.3	846.8	850.4	854.0	857.5	861.0	864.6	868.2	871.8	[c]	[c]	[c]	[c]
235	801.4	816.0	823.4	826.8	830.4	834.0	837.6	844.7	848.2	851.8	855.3	858.8	862.3	865.9	869.5	873.1	[c]	[c]	[c]	[c]
240	804.5	818.9	826.0	829.7	833.3	836.8	840.4	847.5	851.0	854.5	858.0	861.5	865.1	868.6	872.2	[c]	[c]	[c]	[c]	[c]
245	805.7	819.8	826.7	830.1	833.8	837.4	841.0	848.1	851.6	855.2	858.7	862.2	865.8	869.3	[c]	[c]	[c]	[c]	[c]	[c]
250	807.4	821.8	828.9	832.3	835.9	839.4	842.9	849.9	853.4	856.9	860.4	863.9	867.4	870.9	[c]	[c]	[c]	[c]	[c]	[c]

[a]The final boiling point is 5 °C above the initial boiling point for all cuts. [b]Not measured. [c]Freezing induced above the indicated temperature.

https://doi.org/10.1021/acs.energyfuels.2c02625
Energy Fuels 2022, 36, 12563−12579

Table 2. Density of Synthetic Distillate Cuts at All Measured Temperatures[a]

	density at indicated measurement temperatures in °C (kg m^{-3})																			
initial boiling point (°C)	60	40	30	25	20	15	10	0	−5	−10	−15	−20	−25	−30	−35	−40	−45	−50	−55	−60
140	[b]	717.4	725.8	729.7	733.6	737.6	741.4	749.4	753.1	757.0	760.8	764.6	768.5	772.3	776.2	779.9	783.9	787.7	791.5	795.3
145	703.7	720.0	727.9	731.6	735.5	739.4	743.4	751.0	754.9	758.7	762.6	766.3	770.1	773.9	777.8	781.6	785.4	789.2	793.1	796.8
150	705.7	721.7	729.8	733.7	737.6	741.5	745.3	753.0	756.7	760.6	764.4	768.2	772.0	775.8	779.6	783.4	787.2	791.0	794.8	798.5
155	709.8	725.8	733.6	737.4	741.2	745.0	748.8	756.5	760.2	764.0	767.8	771.5	775.2	779.0	782.8	786.6	790.4	794.2	797.9	801.6
160	712.9	728.9	736.6	740.3	744.1	747.9	751.7	759.3	763.0	766.8	770.4	774.0	778.0	781.7	785.5	789.3	793.0	796.8	800.5	804.2
165	715.1	731.0	738.8	742.4	746.2	750.0	753.7	761.3	765.0	768.7	772.4	776.1	779.9	783.6	787.4	791.1	794.9	798.6	802.4	806.1
170	718.6	734.3	742.0	745.7	749.4	753.2	756.9	764.4	768.2	771.9	775.6	779.2	783.0	786.7	790.4	794.2	797.9	801.6	805.4	809.0
175	723.8	739.4	747.0	750.6	754.4	758.1	761.8	769.3	773.0	776.7	780.3	784.0	787.7	791.4	795.1	798.8	802.5	806.2	810.0	813.6
180	726.3	741.7	749.4	752.9	756.6	760.3	764.1	771.5	775.2	778.8	782.5	786.2	789.8	793.5	797.2	800.9	804.6	808.3	812.0	815.7
185	729.1	744.1	751.7	755.5	759.0	762.9	766.7	774.1	777.7	781.4	785.0	788.7	792.3	796.0	799.6	803.3	807.0	810.7	814.4	818.0
190	731.3	746.6	754.1	757.7	761.4	765.1	768.8	776.1	779.8	783.4	787.0	790.7	794.3	798.0	801.6	805.3	809.0	812.7	816.3	820.0
195	733.7	749.0	756.5	760.0	763.7	767.4	771.0	778.4	782.0	785.6	789.3	792.8	796.5	800.1	803.8	807.4	811.1	814.8	818.4	822.0
200	736.2	751.6	759.2	762.7	766.4	770.0	773.7	781.0	784.6	788.2	791.8	795.4	798.7	802.5	806.0	809.7	[b]	[b]	[b]	[b]
205	740.4	755.7	763.2	766.8	770.4	774.1	777.7	785.0	788.6	792.2	795.8	799.5	803.1	806.7	810.3	814.0	817.6	821.3	825.0	[c]
210	741.4	756.1	763.5	767.3	771.0	774.6	778.3	785.4	789.1	792.7	796.3	799.9	803.5	[b]	[b]	[b]	[b]	[b]	[b]	[b]
215	742.4	757.1	764.2	767.9	771.3	774.8	778.4	785.5	789.0	792.5	795.9	799.9	803.6	807.2	810.8	814.4	818.0	821.7	825.3	[c]
220	743.8	758.5	766.0	769.4	773.1	776.7	780.3	787.5	791.0	794.6	798.1	801.7	805.3	808.9	812.5	816.1	819.7	823.3	826.9	[c]
225	744.7	759.6	766.8	770.5	774.1	777.7	781.3	788.5	792.0	795.6	799.1	802.6	806.2	809.8	813.4	817.0	820.6	824.2	[c]	[c]
230	745.8	760.3	767.3	770.9	774.4	777.8	781.2	788.2	791.6	795.1	798.6	802.0	805.5	809.0	812.5	816.0	819.6	823.3	[c]	[c]
235	746.7	761.1	768.3	772.0	775.5	779.1	782.7	789.7	793.3	796.8	800.3	803.8	807.3	810.9	814.4	818.0	821.6	[c]	[c]	[c]
240	747.8	762.2	769.3	773.0	776.5	780.0	783.6	790.6	794.1	797.7	801.1	804.6	808.1	811.7	815.2	818.8	822.3	[c]	[c]	[c]
245	748.7	763.2	770.3	773.9	777.5	781.0	784.5	791.5	795.1	798.6	802.1	805.5	809.0	812.5	816.1	819.6	[c]	[c]	[c]	[c]
250	750.2	764.5	771.6	775.2	778.8	782.3	785.8	792.8	796.3	799.7	803.2	806.7	810.2	813.7	817.2	[c]	[c]	[c]	[c]	[c]
255	751.9	766.3	773.5	776.7	780.3	783.7	787.2	794.1	797.7	801.2	804.6	808.1	811.5	815.0	818.5	[c]	[c]	[c]	[c]	[c]
260	753.2	766.7	774.2	778.0	781.6	785.1	788.6	795.6	796.6	800.0	803.5	806.8	810.3	813.8	817.3	[c]	[c]	[c]	[c]	[c]
265	755.2	769.4	776.4	779.8	783.3	786.8	790.3	797.1	800.6	804.1	807.5	810.9	814.4	817.9	821.4	[c]	[c]	[c]	[c]	[c]
270	757.0	771.0	778.0	781.5	784.9	788.5	791.9	798.8	802.3	805.7	809.2	812.6	816.0	819.5	[c]	[c]	[c]	[c]	[c]	[c]
275	758.7	772.7	779.6	783.2	786.7	790.2	793.6	800.4	803.9	807.4	810.8	814.2	817.6	821.1	[c]	[c]	[c]	[c]	[c]	[c]
280	760.6	774.7	781.7	785.0	788.4	791.9	795.4	802.2	805.6	809.1	812.4	815.9	819.3	[c]	[c]	[c]	[c]	[c]	[c]	[c]
285	762.3	776.2	783.0	786.6	790.0	793.4	796.9	803.7	807.1	810.6	813.9	817.3	820.8	[c]	[c]	[c]	[c]	[c]	[c]	[c]
290	764.2	778.1	785.1	788.4	791.8	795.2	798.7	805.4	808.9	812.3	815.6	819.0	822.4	[c]	[c]	[c]	[c]	[c]	[c]	[c]
295	765.7	779.4	786.2	789.7	793.1	796.5	799.9	806.7	809.9	813.5	816.9	820.3	[c]	[c]	[c]	[c]	[c]	[c]	[c]	[c]
300	767.2	780.8	787.7	791.2	794.5	797.9	801.3	808.1	811.5	814.9	818.3	821.7	[c]	[c]	[c]	[c]	[c]	[c]	[c]	[c]
305	767.7	781.4	788.2	791.8	795.1	798.5	801.9	808.6	812.0	815.3	818.8	[c]	[c]	[c]	[c]	[c]	[c]	[c]	[c]	[c]
310	769.2	782.8	789.6	793.0	796.3	799.7	803.1	809.7	813.2	816.4	819.9	[c]	[c]	[c]	[c]	[c]	[c]	[c]	[c]	[c]
315	770.7	784.2	791.0	794.4	797.7	801.1	804.4	811.0	814.3	817.8	820.8	[c]	[c]	[c]	[c]	[c]	[c]	[c]	[c]	[c]
320	772.3	785.7	792.5	795.8	799.1	802.5	805.8	812.4	815.8	819.1	[c]	[c]	[c]	[c]	[c]	[c]	[c]	[c]	[c]	[c]

[a]The final boiling point is 5 °C above the initial boiling point for all cuts. [b]Not measured. [c]Freezing induced above the indicated temperature.

https://doi.org/10.1021/acs.energyfuels.2c02625
Energy Fuels 2022, 36, 12563−12579

Table 3. Dynamic Viscosity of Petroleum-Based Kerosene Cuts at All Measured Temperatures[a]

initial boiling point (°C)	dynamic viscosity at indicated measurement temperatures in °C (mPa s)																			
	60	40	30	25	20	15	10	0	−5	−10	−15	−20	−25	−30	−35	−40	−45	−50	−55	−60
140	[b]	0.5465	0.6450	0.6871	0.737	0.7909	0.8501	0.9964	1.121	1.235	1.363	1.503	1.677	1.888	2.117	2.404	2.758	3.191	3.733	4.454
145	[b]	0.5566	0.6368	0.6824	0.7336	0.7884	0.8521	0.9969	1.101	1.210	1.340	1.491	1.667	1.873	2.120	2.417	2.782	3.234	3.803	4.530
150	[b]	0.5821	0.6589	0.7062	0.7563	0.8139	0.8820	1.035	1.172	1.294	1.435	1.597	1.789	2.017	2.291	2.624	3.037	3.555	4.212	5.065
155	[b]	0.6357	0.7220	0.7697	0.8248	0.8878	0.9586	1.129	1.276	1.410	1.566	1.749	1.983	2.244	2.559	2.958	3.420	4.024	4.805	5.836
160	[b]	0.6351	0.7271	0.7838	0.8462	0.9161	0.9939	1.172	1.333	1.482	1.670	1.870	2.108	2.397	2.751	3.207	3.742	4.448	5.371	6.615
165	[b]	0.6676	0.7666	0.8273	0.8921	0.9588	1.045	1.257	1.423	1.581	1.770	1.996	2.264	2.586	2.978	3.485	4.087	4.894	5.953	7.413
170	[b]	0.7483	0.8534	0.9177	0.9896	1.071	1.164	1.394	1.580	1.761	1.974	2.230	2.536	2.910	3.372	3.970	4.703	5.675	6.990	8.835
175	[b]	0.7919	0.9098	0.9792	1.059	1.151	1.255	1.512	1.717	1.921	2.165	2.458	2.811	3.247	3.790	4.505	5.380	6.578	8.221	10.56
180	0.6455	0.8337	0.9621	1.041	1.129	1.229	1.344	1.630	1.852	2.080	2.352	2.681	3.081	3.577	4.202	5.032	6.061	7.486	9.473	12.33
185	0.6801	0.8818	1.022	1.107	1.202	1.311	1.437	1.751	1.995	2.247	2.550	2.919	3.370	3.935	4.653	5.614	6.824	8.518	10.91	14.42
190	0.8325	1.023	1.180	1.278	1.390	1.518	1.667	2.043	2.328	2.631	2.997	3.447	3.989	4.694	5.588	6.800	8.354	10.56	13.78	[c]
195	0.7666	1.009	1.178	1.283	1.402	1.539	1.698	2.103	2.406	2.735	3.137	3.633	4.252	5.043	6.073	7.486	9.331	11.99	15.89	[c]
200	0.8109	1.072	1.258	1.372	1.503	1.655	1.833	2.288	2.627	3.001	3.460	4.031	4.752	5.682	6.907	8.611	10.87	14.19	19.13	[c]
205	0.8511	1.132	1.332	1.456	1.599	1.765	1.960	2.460	2.831	3.245	3.755	4.396	5.209	6.267	7.673	9.647	12.29	16.22	22.16	[c]
210	0.8943	1.189	1.407	1.543	1.698	1.879	2.090	2.642	3.047	3.506	4.075	4.793	5.713	6.921	8.542	10.98	13.98	18.69	25.93	[c]
215	0.9404	1.268	1.506	1.655	1.827	2.030	2.268	2.892	3.351	3.879	4.540	5.393	6.478	7.932	9.912	12.91	16.70	22.74	[c]	[c]
220	0.9911	1.343	1.604	1.767	1.957	2.180	2.446	3.144	3.656	4.256	5.012	5.999	7.266	8.983	11.35	14.97	19.67	27.25	[c]	[c]
225	1.048	1.433	1.720	1.901	2.112	2.360	2.655	3.447	4.029	4.719	5.598	6.754	8.260	10.33	13.23	17.72	23.68	[c]	[c]	[c]
230	1.137	1.565	1.888	2.094	2.336	2.624	2.969	3.901	4.587	5.421	6.493	7.919	9.857	12.45	16.19	22.10	[c]	[c]	[c]	[c]
235	1.176	1.635	1.985	2.207	2.471	2.782	3.159	4.186	4.943	5.868	7.069	8.682	10.84	13.87	18.24	25.21	[c]	[c]	[c]	[c]
240	1.251	1.752	2.139	2.387	2.680	3.032	3.459	4.633	5.503	6.582	8.001	9.920	12.52	16.22	21.63	[c]	[c]	[c]	[c]	[c]
245	1.326	1.879	2.309	2.585	2.914	3.310	3.794	5.138	6.141	7.403	9.079	11.37	14.52	19.06	[c]	[c]	[c]	[c]	[c]	[c]
250	1.402	2.005	2.479	2.786	3.153	3.598	4.145	5.685	6.841	8.314	10.28	13.01	16.80	22.35	[c]	[c]	[c]	[c]	[c]	[c]

[a]The final boiling point is 5 °C above the initial boiling point for all cuts; the derived kinematic viscosity, shear rate, and shear stress are summarized in Table S7 of the Supporting Information. [b]Not measured. [c]Freezing induced above the indicated temperature.

https://doi.org/10.1021/acs.energyfuels.2c02625
Energy Fuels 2022, 36, 12563−12579

Table 4. Dynamic Viscosity of Synthetic Distillate Cuts at All Measured Temperatures[a]

initial boiling point (°C)	dynamic viscosity at indicated measurement temperatures in °C (mPa s)																			
	60	40	30	25	20	15	10	0	−5	−10	−15	−20	−25	−30	−35	−40	−45	−50	−55	−60
140	[b]	0.5303	0.6015	0.6422	0.6876	0.7373	0.7948	0.9281	1.043	1.144	1.260	1.397	1.557	1.743	1.965	2.210	2.527	2.918	3.398	3.988
145	0.4336	0.5456	0.6200	0.6642	0.7121	0.7653	0.8247	0.9682	1.088	1.197	1.323	1.469	1.640	1.842	2.083	2.374	2.730	3.171	3.725	4.428
150	0.5037	0.5737	0.6545	0.7001	0.7521	0.8087	0.8730	1.027	1.154	1.275	1.414	1.575	1.763	1.986	2.254	2.582	2.988	3.496	4.138	4.970
155	0.4984	0.6286	0.7175	0.7690	0.8258	0.8895	0.9614	1.135	1.276	1.410	1.565	1.749	1.995	2.255	2.577	2.984	3.475	4.112	4.940	6.050
160	0.5002	0.6387	0.7322	0.7879	0.8494	0.9185	0.9966	1.187	1.337	1.480	1.653	1.862	2.104	2.398	2.756	3.218	3.767	4.499	5.465	6.779
165	0.5220	0.6667	0.7654	0.8244	0.8896	0.9633	1.047	1.251	1.413	1.571	1.756	1.979	2.245	2.567	2.964	3.479	4.097	4.927	6.038	7.569
170	0.5474	0.7043	0.8115	0.8757	0.9470	1.027	1.119	1.345	1.516	1.694	1.902	2.149	2.451	2.816	3.269	3.865	4.586	5.566	6.892	8.749
175	0.5922	0.7640	0.8837	0.9564	1.038	1.130	1.235	1.494	1.692	1.895	2.140	2.435	2.793	3.237	3.795	4.536	5.453	6.742	8.504	[b]
180	0.6132	0.7961	0.9228	0.9994	1.085	1.183	1.296	1.576	1.790	2.011	2.277	2.599	2.993	3.486	4.108	4.940	5.980	7.431	9.459	12.40
185	0.6368	0.8380	0.9756	1.057	1.151	1.257	1.379	1.685	1.918	2.163	2.459	2.821	3.264	3.822	4.535	5.498	6.717	8.435	10.87	14.44
190	0.6732	0.8822	1.029	1.118	1.219	1.335	1.469	1.808	2.060	2.330	2.660	3.064	3.564	4.200	5.017	6.131	7.561	9.597	12.52	16.90
195	0.7063	0.9302	1.088	1.185	1.295	1.421	1.567	1.941	2.216	2.517	2.883	3.339	3.906	4.633	5.574	6.870	8.555	10.99	14.53	19.87
200	0.7668	1.019	1.201	1.310	1.434	1.578	1.744	2.170	2.484	2.834	3.263	3.799	4.467	5.322	6.458	8.040	[b]	[b]	[b]	[b]
205	0.7641	1.014	1.192	1.299	1.422	1.568	1.736	2.166	2.488	2.845	3.282	3.831	4.523	5.423	6.605	8.254	10.45	13.66	18.44	
210	0.8186	1.090	1.288	1.406	1.545	1.704	1.895	2.384	2.740	3.146	3.649	4.284	5.096	[b]	[b]	[b]	[b]	[b]	[b]	[b]
215	0.8307	1.118	1.324	1.451	1.599	1.770	1.970	2.494	2.877	3.315	3.863	4.566	5.449	6.621	8.197	10.56	13.49	18.05	24.97	[c]
220	0.8725	1.180	1.403	1.542	1.704	1.892	2.114	2.695	3.118	3.611	4.230	5.027	6.043	7.406	9.260	12.07	15.59	21.16	29.74	[c]
225	0.9179	1.247	1.489	1.641	1.818	2.024	2.268	2.913	3.385	3.940	4.639	5.551	6.721	8.304	10.48	13.80	18.05	24.82	[c]	[c]
230	0.9730	1.332	1.601	1.768	1.962	2.192	2.470	3.203	3.739	4.378	5.192	6.260	7.649	9.547	12.19	16.25	21.55	30.09	[c]	[c]
235	1.020	1.409	1.700	1.884	2.099	2.353	2.658	3.474	4.072	4.792	5.715	6.939	8.541	10.76	13.85	18.67	25.04	[c]	[c]	[c]
240	1.081	1.501	1.819	2.021	2.260	2.543	2.883	3.807	4.483	5.308	6.376	7.797	9.681	12.32	16.04	21.87	29.70	[c]	[c]	[c]
245	1.134	1.586	1.932	2.153	2.413	2.723	3.099	4.126	4.878	5.806	7.012	8.635	10.81	13.86	18.20	25.06	[c]	[c]	[c]	[c]
250	1.202	1.698	2.081	2.325	2.615	2.963	3.384	4.550	5.405	6.476	7.877	9.777	12.35	15.98	21.21	[c]	[c]	[c]	[c]	[c]
255	1.276	1.814	2.234	2.505	2.827	3.217	3.691	5.017	5.990	7.220	8.849	11.07	14.09	18.41	24.72	[c]	[c]	[c]	[c]	[c]
260	1.338	1.919	2.387	2.672	3.019	3.444	3.964	5.422	6.523	7.905	9.742	12.27	15.73	20.72	28.04	[c]	[c]	[c]	[c]	[c]
265	1.403	2.025	2.516	2.835	3.218	3.683	4.255	5.867	7.068	8.607	10.68	13.52	17.45	23.15	31.54	[c]	[c]	[c]	[c]	[c]
270	1.483	2.153	2.689	3.039	3.460	3.974	4.609	6.412	7.764	9.510	11.86	15.11	19.68	26.31	[c]	[c]	[c]	[c]	[c]	[c]
275	1.555	2.274	2.851	3.230	3.688	4.248	4.943	6.932	8.430	10.38	13.01	16.68	21.87	29.44	[c]	[c]	[c]	[c]	[c]	[c]
280	1.654	2.445	3.086	3.510	4.023	4.654	5.442	7.714	9.439	11.70	14.79	19.10	25.26	[c]	[c]	[c]	[c]	[c]	[c]	[c]
285	1.752	2.606	3.307	3.772	4.337	5.036	5.911	8.457	10.40	12.97	16.49	21.50	28.57	[c]	[c]	[c]	[c]	[c]	[c]	[c]
290	1.860	2.798	3.571	4.088	4.719	5.503	6.490	9.383	11.61	14.57	18.67	24.52	32.87	[c]	[c]	[c]	[c]	[c]	[c]	[c]
295	1.972	2.993	3.840	4.409	5.107	5.973	7.077	10.33	12.87	16.24	20.93	27.68	[c]	[c]	[c]	[c]	[c]	[c]	[c]	[c]
300	2.060	3.151	4.063	4.677	5.432	6.377	7.576	11.15	13.93	17.66	22.90	30.44	[c]	[c]	[c]	[c]	[c]	[c]	[c]	[c]
305	2.179	3.348	4.337	5.007	5.834	6.873	8.197	12.16	15.27	19.47	25.38	[c]	[c]	[c]	[c]	[c]	[c]	[c]	[c]	[c]
310	2.357	3.673	4.802	5.567	6.518	7.718	9.262	13.94	17.63	22.66	29.78	[c]	[c]	[c]	[c]	[c]	[c]	[c]	[c]	[c]
315	2.500	3.938	5.177	6.025	7.084	8.426	10.16	15.44	19.64	25.40	44.78	[c]	[c]	[c]	[c]	[c]	[c]	[c]	[c]	[c]
320	2.774	4.443	5.904	6.912	8.180	9.800	11.90	18.40	23.64	30.89	[c]	[c]	[c]	[c]	[c]	[c]	[c]	[c]	[c]	[c]

[a]The final boiling point is 5 °C above the initial boiling point for all cuts; derived kinematic viscosity, shear rate, and shear stress are summarized in Table S8 of the Supporting Information. [b]Not measured. [c]Freezing induced above the indicated temperature.

https://doi.org/10.1021/acs.energyfuels.2c02625
Energy Fuels 2022, 36, 12563−12579

Table 5. Characteristic Points in DSC Curves and Optically Determined Freezing Point of Narrow Boiling Range Distillation Cuts of Petroleum-Based Kerosene[a]

initial boiling point (°C)	DSC onset of freezing (°C)[b]	DSC end of melting endotherm (°C)[b]	freezing point, optical determination (°C)[c]	enthalpy of phase change during freezing (J g^{-1})	enthalpy of phase change during melting (J g^{-1})
200	−60.0	−46.1	−46	−9	12
205	−59.1	−44.2	−43	−14	14
210	−55.4	−40.7	−41	−11	14
215	−52.3	−38.2	−38	−22	20
220	−51.4	−40.1	−40	−22	22
225	−49.8	−42.7	−43	−18	18
230	−45.0	−37.4	−37	−20	23
235	−42.3	−35.5	−35	−25	26
240	−40.7	−29.8	−29	−27	28
245	−37.8	−24.6	−26	−29	30
250	−33.1	−21.2	−21	−33	32

[a]The final boiling point is 5 °C above the initial boiling point; for distillation cuts with an initial boiling point below 200 °C, and freezing was not induced at −70 °C. [b]See Figure 1. [c]Optical determination of wax crystal dissolution (see the Section 2). Reproducibility of the method is ±1.3 °C according to the instrument manufacturer; therefore, the first decimal is omitted.

Table 6. Characteristic Points in DSC Curves and Optically Determined Freezing Point of Narrow Boiling Range Distillation Cuts of Synthetic Distillate[a]

initial boiling point (°C)	DSC onset of freezing (°C)[b]	DSC end of melting endotherm (°C)[b]	freezing point, optical determination (°C)[c]	enthalpy of phase change during freezing (J g^{-1})	enthalpy of phase change during melting (J g^{-1})
195	[d]	−62.2	[e]	[c]	9
200	−66.1	−56.0	−57	−7	11
205	−60.4	−47.5	−48	−10	11
210	−58.1	−43.2	−43	−9	13
215	−57.5	−41.3	−41	−15	15
220	−57.0	−41.0	−41	−14	15
225	−55.6	−46.5	−47	−19	20
230	−53.7	−42.7	−43	−17	19
235	−50.8	−39.1	−41	−16	19
240	−47.7	−37.2	−37	−17	19
245	−47.5	−30.8	−30	−21	22
250	−42.7	−25.6	−25	−20	21
255	−41.7	−25.4	−25	−18	20
260	−40.7	−31.2	−31	19	21
265	−35.7	−26.6	−27	−16	21
270	−34.1	−24.6	−25	−17	21
275	−33.2	−23.8	−23	−22	22
280	−31.2	−21.0	−20	−23	23
285	−29.3	−18.6	−18	−24	24
290	−26.9	−17.7	−17	−24	26
295	−25.7	−15.4	−15	−23	23
300	−22.8	−14.8	−15	−24	23
305	−21.9	−11.6	−11	−24	25
310	−16.3	−10.3	−10	−23	25
315	−16.4	−7.9	−7	−24	25
320	−11.9	−3.9	−4	−27	25

[a]The final boiling point is 5 °C above the initial boiling point; for samples with boiling point below 195 °C, freezing was not induced. [b]See Figure 1. [c]Optical determination of wax crystal dissolution (see the Section 2). Reproducibility of the method is ±1.3 °C according to the instrument manufacturer; therefore, the first decimal is omitted. [d]Freezing induced during hold time at −70 °C. [e]Cooling insufficient to induce freezing.

Compared to the measured value, this is a relative uncertainty around 10−15%.

4. DISCUSSION

4.1. Temperature Dependence of Viscosity. As pointed out in the Introduction, a kinematic viscosity of <12 mm^2 s^{-1} needs to be ensured at −40 °C for jet fuels, but jet fuel standards such as ASTM D1655[2] and ASTM D7566[4] have specifications for viscosity at −20 °C for petroleum-based and some semi-synthetic jet fuels. The specification indirectly implies that if a fuel fulfills the regulated viscosity of <8 mm^2 s^{-1} at −20 °C, it is fit-for-purpose, meaning that its viscosity will remain below 12 mm^2 s^{-1} under in-flight conditions, which can include temperatures down to −40 °C. This implies that the viscosity of any jet fuel has the same temperature dependence. With the introduction of synthetic fuels such as the various types of SPK, it is important to confirm that the temperature dependence of viscosity is really very similar or the same as for petroleum-based fuels. This is of particular importance when these fuels are used as fully synthetic fuels, i.e., without blending with a petroleum-based material. The suggested kinematic viscosity−temperature dependence for jet fuels is eq 1.[5] The kinematic viscosity, calculated from dynamic viscosity and density, is regulated in ASTM D7566, not the dynamic viscosity.

4.1.1. Viscosity−Temperature Dependence of Narrow Distillate Cuts. To determine whether SPK-type fuels produced via hydrocracking follow the same viscosity−temperature dependence, it was investigated whether eq 1 describes the kinematic viscosity−temperature behavior for hydrocracking-derived SPK-type fuels such as the synthetic distillate cuts with the same accuracy as for petroleum-based kerosene cuts.

For both the petroleum-based kerosene cuts and the synthetic distillate cuts and without any exceptions, the dynamic viscosity decreases monotonically with increasing measurement temperature (Tables 3 and 4).

The parameters for MacCoull's equation (eq 1) were determined for all cuts, using all recorded viscosity data to fit the parameters. The kinematic viscosity was calculated for this purpose (Tables S7 and S8). The kinematic viscosities predicted from the equation using the determined parameters matched the experimental data with a maximum relative deviation of 5.0% for the petroleum-based kerosene cuts and 4.0% for the synthetic distillate cuts, respectively (see Tables 7 and 8). The relationship describes the viscosity−temperature behavior acceptably, despite the broad temperature range for which the data was collected and despite the viscosity data near the freezing point being included in the data set. Close to the freezing point, structural changes in the fluid can lead to an increase of the viscosity with temperature that is steeper than the exponential increase that is observed at higher temperatures.[25] From the fact that the deviation between predicted and experimental kinematic viscosity is lower for the synthetic kerosene cuts than for the petroleum-based kerosene cuts, it can be concluded that the viscosity−temperature behavior of the synthetic distillate is similar to that of petroleum-based kerosene.

The values in Tables 7 and 8 only demonstrate that MacCoull's equation (eq 1) applies equally to petroleum and synthetic narrow cuts. The value of this observation is that it shows that the claim made by Moses and Roets[7] for petroleum and synthetic broad cut kerosene fractions also applies to the

https://doi.org/10.1021/acs.energyfuels.2c02625
Energy Fuels 2022, 36, 12563−12579

Table 7. Petroleum-Based Kerosene Cuts: Parameters *A* and *B* from MacCoull's Viscosity−Temperature Equation Used in ASTM D341, Maximum Relative Deviation between the Kinematic Viscosity Predicted via ASTM D341 and Experimental Data as well as r^2 of the Correlation

initial boiling point (°C)	minimum viscosity determination temperature (°C)	maximum viscosity determination temperature (°C)	*A*	*B*	maximum relative deviation between predicted and experimental data (%)	r^2
140	−60	40	9.110	3.953	5.0	0.99858
145	−60	40	9.201	3.993	3.8	0.99919
150	−60	40	9.364	4.053	4.5	0.99888
155	−60	40	9.244	3.991	3.6	0.99917
160	−60	40	9.569	4.120	4.8	0.99895
165	−60	40	9.569	4.111	4.3	0.99920
170	−60	40	9.332	3.999	1.7	0.99983
175	−60	40	9.528	4.068	1.5	1.00000
180	−60	60	9.437	4.022	1.2	0.99994
185	−60	60	9.458	4.022	1.1	0.99994
190	−60	40	9.023	3.824	5.6	0.99964
195	−55	60	9.561	4.043	0.8	0.99995
200	−55[a]	60	9.623	4.059	1.4	0.99991
205	−55[a]	60	9.642	4.060	1.9	0.99985
210	−55[a]	60	9.672	4.064	2.5	0.99978
215	−50[a]	60	9.686	4.061	0.7	1.00000
220	−35	60	9.783	4.092	2.5	0.99998
225	−45[a]	60	9.997	4.170	3.8	0.99626
230	−40[a]	60	9.843	4.096	3.8	0.99995
235	−40[a]	60	9.911	4.118	4.0	0.99994
240	−30[a]	60	9.899	4.105	1.6	0.99999
245	−30[a]	60	9.943	4.114	1.9	0.99999
250	−30[a]	60	10.007	4.132	2.1	0.99998

[a]Viscosity measurement at temperatures slightly below the optically determined freezing point is possible because the onset of freezing was not reached at that temperature.

individual constituent narrow cuts in that boiling range. The implication of the present work is that broadening or narrowing the distillation range of synthesized paraffinic kerosene for use as a jet fuel blending component will not affect the ability to describe the viscosity−temperature in terms of ASTM D341.[5]

The numerical values of *A* and *B* in eq 1 as noted in Tables 7 and 8, despite their implied physical meaning, are sensitive to the numerical regression. They do describe the shape of the viscosity−temperature curve, but the three logarithmic functions in the equation make it ill-advised to infer anything based on the fitting parameters *A* and *B*.

4.1.2. Viscosity−Temperature Dependence of Wide-Boiling Kerosenes and Jet Fuel. To gain additional confidence in the generalization of the statement that petroleum and synthetic kerosene fractions are similarly described by ASTM D341,[5] as claimed in ref 7, the evaluation was expanded to other viscosity−temperature data sets. For reference, the parameters for MacCoull's equation have been determined for different petroleum and synthetic kerosene fractions reported in the literature (Table 9).[6,10−12,26−32]

The collected data in Table 9 is of data sets of varying temperature ranges and numbers of points used for the correlation. The correlation coefficient is used as a rough indicator for the goodness-of-fit to MacCoull's equation. The correlation coefficient r^2 for MacCoull's viscosity−temperature relationship for most data sets is >0.998. No systematic difference in the goodness-of-fit was seen between petroleum-derived and synthetic kerosene fractions. The synthetic kerosene fractions included in Table 9 span a wide range of starting materials and methods of preparation as outlined in the appendixes of ASTM D7566.[4] No evidence was found in Tables 7−9 to indicate that there was a difference in the applicability of ASTM D341[5] to kerosene fractions prepared specifically for use as a jet fuel, irrespective of origin.

4.1.3. Estimation of Viscosity Using MacCoull's Equation. The application of MacCoull's equation to predict the kinematic viscosity of kerosene fractions at low-temperature conditions from measurements performed at higher temperatures is particularly useful because experimental data for viscosity at cold temperatures is not always readily available.[33] It was repeatedly pointed out that low-temperature viscosity data is critically important for kerosene intended for use as jet fuel. Hence, it was of interest to determine how accurately the low-temperature viscosity behavior could be estimated using MacCoull's equation, from data obtained at higher temperatures. By its very nature, this is an extrapolation, and the concerns raised in Section 4.1.1 about the sensitivity of fitting parameters *A* and *B* to the regression were central to this concern.

Due to the limited availability of data for wide-boiling kerosenes, the analysis was carried out with the narrow cuts of petroleum-based kerosene and synthetic distillate (see Section 2.1). The parameters of all cuts for MacCoull's equation were determined using only data that was acquired at temperatures at or above −20 °C. Then, the kinematic viscosity of the cuts at −40 °C was estimated by extrapolating MacCoull's equation using the determined parameters. The estimated viscosities were compared to the experimentally determined viscosities at −40 °C. This represents a situation when viscosity is only measured down to −20 °C, as is currently required by jet fuel specifications, such as ASTM D1655[2] and several of the synthetic kerosene types in the appendixes of ASTM D7566.[4]

https://doi.org/10.1021/acs.energyfuels.2c02625
Energy Fuels 2022, 36, 12563−12579

Table 8. Synthetic Distillate Cuts: Parameters *A* and *B* from MacCoull's Kinematic Viscosity−Temperature Equation Used in ASTM D341, Maximum Relative Deviation between the Kinematic Viscosity Predicted via ASTM D341 and Experimental Data as well as r^2 of the Correlation

initial boiling point (°C)	minimum viscosity determination temperature (°C)	maximum viscosity determination temperature (°C)	*A*	*B*	maximum relative deviation between predicted and experimental data (%)	r^2
140	−60	40	9.009	3.916	4.0	0.99868
145	−60	60	9.177	3.979	3.1	0.99904
150	−60	40	9.158	3.962	4.1	0.99930
155	−60	60	9.144	3.942	2.4	0.99968
160	−60	60	9.343	4.018	2.7	0.99964
165	−60	60	9.367	4.021	2.2	0.99970
170	−60	60	9.397	4.023	1.7	0.99977
175	−60	60	9.464	4.037	0.9	0.99990
180	−60	60	9.501	4.046	1.0	0.99990
185	−60	60	9.540	4.054	0.9	0.99994
190	−60	60	9.581	4.062	0.8	0.99997
195	−60	60	9.619	4.070	0.8	0.99998
200	−50	60	9.478	3.999	0.8	0.99996
205	−50[a]	60	9.650	4.070	1.1	0.99997
210	−50[a]	60	9.552	4.019	0.8	0.99996
215	−50[a]	60	9.735	4.090	1.5	0.99993
220	−50[a]	60	9.776	4.099	2.1	0.99991
225	−50[a]	60	9.789	4.096	1.9	0.99988
230	−50[a]	60	9.826	4.102	2.0	0.99989
235	−45[a]	60	9.836	4.098	2.4	0.99983
240	−45[a]	60	9.856	4.098	2.5	0.99984
245	−40[a]	60	9.858	4.092	2.8	0.99968
250	−35[a]	60	9.841	4.076	1.2	0.99995
255	−35[a]	60	9.851	4.073	1.2	0.99996
260	−35[a]	60	9.858	4.069	1.1	0.99997
265	−35[a]	60	9.848	4.059	1.1	0.99997
270	−30[a]	60	9.825	4.043	1.1	0.99996
275	−30[a]	60	9.818	4.035	1.1	0.99997
280	−25[a]	60	9.809	4.023	0.8	0.99998
285	−25[a]	60	9.789	4.009	0.8	0.99998
290	−25[a]	60	9.785	4.001	0.7	0.99998
295	−20[a]	60	9.756	3.982	0.8	0.99997
300	−20[a]	60	9.750	3.975	0.7	0.99998

[a]Viscosity measurement at temperatures slightly below the measured optically determined freezing point is possible because the onset of freezing was not reached at that temperature.

To evaluate viscosity performance at temperatures <−20 °C, which is of practical importance for safety, such lower-temperature data needs to be estimated.

Generally, the prediction of viscosity with MacCoull's equation describes the viscosity−temperature behavior well. However, with decreasing temperature, some deviation between experimental and predicted kinematic viscosity can be observed (see Figure S3 in the Supporting Information). The relative difference between the predicted and the experimentally determined kinematic viscosities at −40 °C is shown in Figure 2; the data set is presented in Tables S9 and S10 in the Supporting Information. When data down to −20 °C is available, the maximum difference between the estimated and the measured kinematic viscosity at −40 °C is 6.6%. The deviation is similar for the petroleum-based kerosene cuts as for the synthetic distillate cuts. ASTM D341 does not specify any uncertainty associated with estimating viscosities.[5] The reproducibility of the experimental determination of kinematic viscosity for jet fuels at −40 °C is 2.1% according to ASTM D7042.[9] The extrapolation of MacCoull's equation using measured data down to only −20 °C for the prediction of viscosity at −40 °C therefore exceeds the acceptable error based on the uncertainty stated in ASTM D7042.

Figure 2 shows that there is an increasing bias toward underestimation of the measured kinematic viscosity with increasing boiling point, with few outliers. The freezing point increases with increasing boiling point. It has been pointed out that for many hydrocarbons near the freezing point, the viscosity−temperature correlation does not follow an exponential decay but more complex relationships.[25,34] This is due to the increased packing density under these conditions. The onset temperature and magnitude of this deviation are influenced by the molecular structure.[25,34]

Figure 2 is based on a limited data set, and therefore, the observation cannot be generalized to the use of eq 1 for other materials. Nevertheless, Figure 2 shows that there is a risk of bias involved when using eq 1 for the prediction of viscosity at −40 °C by extrapolating data measured at ≥−20 °C. The progression of the relative deviation versus boiling point is similar for the synthetic and petroleum-based materials, further substantiating that eq 1 describes the kinematic viscosity−

https://doi.org/10.1021/acs.energyfuels.2c02625
Energy Fuels 2022, 36, 12563−12579

Table 9. Parameters *A*, *B*, and the Correlation Coefficient for the Kinematic Viscosity Estimation According to ASTM D341 for Petroleum-Based and Synthetic Kerosenes[a]

fuel type	comment fuel type/origin	ref	minimum viscosity determination temperature (°C)	maximum viscosity determination temperature (°C)	number of viscosity datapoints	*A*	*B*	r^2
Jet A	USA	6	−40	20	3	9.562	4.047	0.99975
Jet A	USA	6	−40	20	3	9.340	3.928	0.99996
Jet A	USA	6	−40	20	3	9.561	4.030	0.99999
Jet A	USA	6	−40	20	3	9.465	3.974	0.99855
Jet A	USA	6	−40	20	3	9.438	3.956	0.99948
Jet A	USA	6	−40	20	3	9.447	3.992	0.99977
Jet A	USA	6	−40	20	3	9.620	4.048	0.99965
Jet A	USA	6	−40	20	3	9.489	4.009	0.99966
Jet A	USA	6	−40	20	3	9.468	3.993	0.99990
Jet A	USA	6	−40	20	3	9.258	3.908	0.99994
Jet A	USA	6	−40	20	3	8.885	3.754	0.99680
Jet A	USA	6	−40	20	3	8.892	3.761	0.99589
Jet A	Canada	6	−40	20	3	8.714	3.703	0.99925
Jet A[b]	reference jet fuel, POSF 10325	28	−40	100	4	9.893	4.186	0.98140
Jet A	Jet A 3602	12	20	100	17	8.918	3.770	0.99976
Jet A	Jet A 3638	12	20	100	17	8.798	3.741	0.99988
Jet A	Jet A 4658	12	20	100	17	8.973	3.790	0.99978
Jet A-1	Canada	6	−40	20	3	9.138	3.881	0.99757
Jet A-1	Canada	6	−40	20	3	9.371	3.948	0.99837
Jet A-1	Canada	6	−40	20	3	9.235	3.899	0.99952
Jet A-1	Canada	6	−40	20	3	8.869	3.744	0.99911
Jet A-1	Canada	6	−40	20	3	9.370	3.941	0.99773
Jet A-1	Canada	6	−40	20	3	8.821	3.738	0.99971
Jet A-1	Latin America	6	−40	20	3	8.412	3.565	0.99999
Jet A-1	Europe	6	−40	20	3	9.349	3.968	0.99990
Jet A-1	Europe	6	−40	20	3	8.948	3.806	0.99945
Jet A-1	Europe	6	−40	20	3	10.115	4.288	0.99966
Jet A-1	Europe	6	−40	20	3	9.103	3.877	0.99977
Jet A-1	Europe	6	−40	20	3	8.884	3.780	0.99968
Jet A-1	Europe	6	−40	20	3	9.348	3.977	0.99968
Jet A-1	Europe	6	−40	20	3	9.545	4.057	1.00000
Jet A-1	Europe	6	−40	20	3	9.291	3.944	0.99977
Jet A-1	Europe	6	−40	20	3	9.229	3.918	0.99627
Jet A-1	Europe	6	−40	20	3	8.679	3.698	0.99727
Jet A-1	Europe	6	−40	20	3	8.891	3.774	1.00000
Jet A-1	Europe	6	−40	20	3	9.100	3.878	0.99865
Jet A-1	South Africa, semi-synthetic	6	−40	20	3	9.294	3.930	0.99961
Jet A-1	South Africa, fully synthetic	6	−40	20	3	9.326	3.929	0.99950
Jet A-1	Middle East	6	−40	20	3	9.704	4.121	0.99989
Jet A-1	Asia	6	−40	20	3	9.446	4.017	0.99981
Jet A-1	Asia	6	−40	20	3	9.409	4.003	0.99873
Jet A-1	Australia	6	−40	20	3	10.389	4.409	0.99988
Jet A-1	Asia	6	−40	20	3	9.318	3.956	0.99993
Jet A-1	Australia	6	−40	20	3	9.406	3.991	0.99997
Jet A-1	Australia	6	−40	20	3	9.048	3.868	0.99531
Jet A-1		27	−40	93	6	9.513	3.982	0.99965
JP-8	USA	6	−40	20	3	9.392	3.978	0.99956
JP-8	USA	6	−40	20	3	9.080	3.852	0.99870
JP-8	USA	6	−40	20	3	9.180	3.884	0.99920
JP-8	USA	6	−40	20	3	9.249	3.905	0.99843
JP-8	USA	6	−40	20	3	9.311	3.930	0.99920
JP-8	USA	6	−40	20	3	9.259	3.932	0.99999
JP-8	USA	6	−40	20	3	9.489	4.009	0.99966
JP-5	USA	6	−40	20	3	9.746	4.087	0.99975
JP-5	USA	6	−40	20	3	9.415	3.953	0.99884
JP-8	USA	6	−40	20	3	8.987	3.806	0.99739
JP-8	USA	6	−40	20	3	9.206	3.894	0.99985
JP-8	USA	6	−40	20	3	9.516	3.993	0.99994
JP-8[b]	reference jet fuel, POSF 10264	28	−40	100	4	9.898	4.213	0.98362
JP-5[b]	reference jet fuel. POSF 10289	28	−40	100	4	10.067	4.229	0.98273

https://doi.org/10.1021/acs.energyfuels.2c02625
Energy Fuels 2022, 36, 12563−12579

Table 9. continued

fuel type	comment fuel type/origin	ref	minimum viscosity determination temperature (°C)	maximum viscosity determination temperature (°C)	number of viscosity datapoints	A	B	r^2
JP-5[b]		29	−40	40	5	10.566	4.444	0.99320
JP-5		30	-20	60	4	9.614	4.049	0.99996
semi-synthetic jet fuel[b]	50% Sasol GTL2, 50% Jet A	11	−40	40	3	9.414	3.963	0.99997
semi-synthetic jet fuel[b]	50% Syntroleum S-8, 50% JP-8	11	−40	40	3	9.548	4.033	0.99919
semi-synthetic jet fuel[b]	50% Sasol IPK, 50% Jet A-1	11	−40	-20	2	8.846	3.747	1.00000
semi-synthetic jet fuel[b]	50% Sasol GTL 1, 50% Jet A	11	−40	40	3	9.199	3.924	0.99987
semi-synthetic jet fuel[b]	10% SIP, 90% JP-5	29	−40	40	4	10.320	4.334	0.99483
semi-synthetic jet fuel[b]	50% HEFA-SPK, 50% JP-5	29	−40	40	5	10.383	4.365	0.99485
semi-synthetic jet fuel	50% Syntroleum S-8, 50% Jet A	31	−40	100	36	9.371	3.947	0.99486
test fuel[b]	84% C14 isoparaffins, 16% 1,3,5-trimethylbenzene, POSF 12223	26	−40	25	3	9.820	4.131	0.99962
test fuel[b]	64% JP-5, 36% farnesane, POSF 12341	26	−20	25	3	9.792	4.086	0.99844
test fuel[b]	60% Sasol IPK, 40% Gevo alcohol to jet fuel, POSF 12344	26	−20	25	3	8.990	3.818	0.99897
test fuel[b]	74% C10 isoparaffins, 16% 1,3,5-trimethylbenzene, POSF 12345	26	−20	25	3	10.593	4.558	0.99746
fully synthetic kerosene[b]	Gevo alcohol to jet fuel, POSF 11498	26	−40	40	4	8.894	3.750	0.99981
fully synthetic kerosene	FT-BUFF "JP-8"	10	−20	40	3	11.093	4.716	0.99646
fully synthetic kerosene	Syntroleum S-8	12	20	100	17	8.835	3.748	0.99966
fully synthetic kerosene	shell GTL	12	20	100	17	8.611	3.715	0.99989
fully synthetic kerosene	Sasol IPK (coal based)	12	20	100	17	8.840	3.773	0.99979
fully synthetic kerosene	cellular synthetic kerosene (isoprenoids from fermentation)	12	20	100	17	8.699	3.742	0.99996
fully synthetic kerosene	HEFA-SPK (camelina oil)	12	20	100	17	8.700	3.719	0.99966
fully synthetic kerosene	HEFA-SPK (castor oil)	12	20	100	17	9.031	3.817	0.99973

[a]The parameters are calculated from the original data given in the reference; the maximum and minimum temperatures and the number of data points used for the regression of A and B are shown. [b]Viscosity data was extracted from a figure because numerical data was not available.

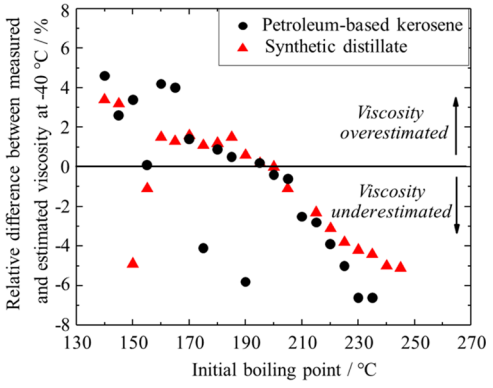

Figure 2. Relative difference between the kinematic viscosity measured at −40 °C and estimated from viscosity data above −20 °C using eq 1 as a function of the initial boiling point of the petroleum-based kerosene cuts and the synthetic distillate cuts. The final boiling point was 5 °C above the initial boiling point. Positive differences indicate an overestimation of the viscosity by eq 1, whereas negative values indicate an underestimation. The full data set is presented in Tables S9 and S10 in the Supporting Information.

temperature relationship of synthetic and petroleum-based materials with similar accuracy.

4.2. Viscosity−Boiling Point Dependence. The dynamic and kinematic viscosities of both the petroleum-based kerosene (Tables 3 and S7) and the synthetic distillate (Tables 4 and S8) increase for cuts with increasing boiling point at all measured temperatures. The progression of dynamic viscosity versus boiling point plots (see Figure 3) is smooth and monotonical and the shape is in line with observations for petroleum cuts,[35,36] pure hydrocarbons,[35] and other pure compounds.[37] Figure 3 suggests that the boiling point and molar mass dependence of the viscosity of SPK-type kerosenes derived from hydrocracking is fundamentally the same as for petroleum-derived kerosenes.

A simple exponential fit ($y = A{\cdot}e^{Bx}$) describes the dynamic viscosity as a function of the molar mass (estimated via eq S2 in the Supporting Information) for all but one distillation cut of both synthetic and petroleum-based materials with a maximum deviation of less than 6% (see Figure 3b). This indicates that within each of the materials, the compound class composition does not change drastically between cuts with different boiling points, but the viscosity increase with boiling point is dominated by molecular dimensions (molar mass).[34]

https://doi.org/10.1021/acs.energyfuels.2c02625
Energy Fuels 2022, 36, 12563−12579

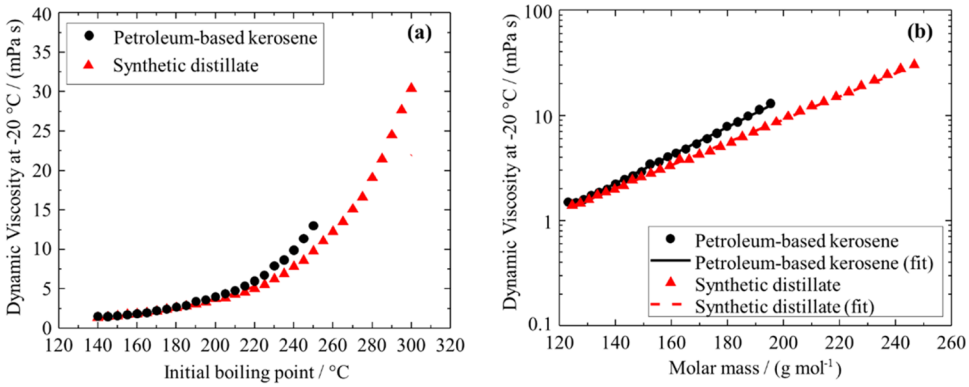

Figure 3. Dynamic viscosity at −20 °C of the petroleum-based kerosene cuts and the synthetic distillate cuts as a function of the initial boiling point (a) and the molar mass estimated by eq S2 in the Supporting Information (b). (b) uses a logarithmic scaling on the ordinate. All fits are the best fits of equations of the form $y = A \cdot e^{Bx}$.

The impact of the molecular structure is apparent when comparing the viscosity of the synthetic distillate and petroleum-based kerosene cuts of the same molar mass. The higher viscosity of the petroleum-based kerosene is likely caused by the higher content of cyclic hydrocarbons such as aromatics (see Figure S2) and cycloalkanes. These molecules typically exhibit higher viscosities than *n*- and iso-alkanes with similar or the same molar mass or boiling point.[25,38−40] *N*- and iso-alkanes are the predominant compound class of the synthetic distillate.[14]

For blending of fuel products such as jet fuel, the cut points determine the viscosity of the fuel. When comparing both tested materials, the increase in viscosity with boiling point is larger for the petroleum-based kerosene than for the synthetic distillate (see Figure 3). This implies that for the same boiling cut range, the petroleum-based kerosene is more likely to exceed viscosity specifications than the synthetic distillate. This is left as an empirical observation, and there is not enough evidence to generalize this finding to other materials than the ones investigated in this study.

4.3. Refractive Index and Density. The density and refractive index are shown together (Figure 4) because they are both parameters affecting the molar refractivity (eq S1 in the Supporting Information). Molar refractivity is a sum of the bond refraction values and therefore a measure of composition.[20,41] With the same compound class composition, one would anticipate the refractive index and density to change in tandem, following a nonlinear relationship that is defined by eq S1. The calculated molar refractivity (see Tables S5 and S6) increases linearly with the estimated molar mass of the fractions of both materials with correlation coefficients higher than 0.999 for both materials. This indicates that there was little compound class variability over the boiling range. This corroborates the observation in Section 4.2 that the increase of viscosity at a constant temperature with increasing boiling point (Figure 3) was mainly determined by the molecular dimensions and less by compound class compositional changes.

The relation between density and temperature for each cut is linear (see Section 3.2). New synthetic fuel candidates must show such a linear relationship as part of the fit-for-purpose investigation in ASTM D4054.[9] For both materials, the increase in density with boiling point is not linear but exhibits changes in the slope (Figure 4). A similar behavior is apparent for the synthetic distillate cuts. The nonlinearities observed for both materials have also been reported for crude oil distillation fractions with broader boiling ranges as well as hydrocarbon condensate cuts.[21,23,42,43]

For the petroleum distillate, the nonlinearities of density versus boiling point in the ranges 150−180 and 210−225 °C coincide with the local minima in the aromatic volume fraction as a function of the boiling point (see Figure S2). The trend is consistent with the higher density of aromatics compared to alkanes.[44] Despite the changes in the volume fraction of aromatics, which represent compound class compositional changes, the dynamic viscosity increased with molar mass without nonlinearities (see Figure 3b). Hence, with an increase in the boiling range of one type of material, the impact of molecular dimension (molar mass) on viscosity was much more pronounced than compound class compositional changes. The density, on the other hand, was affected by both changes in the molar mass and compound class compositional changes between different cuts of petroleum kerosene. For the synthetic distillate that was a product of wax hydrocracking, a similar HPLC analysis was not carried out in this study, as the aromatic mass fraction is very low.[14]

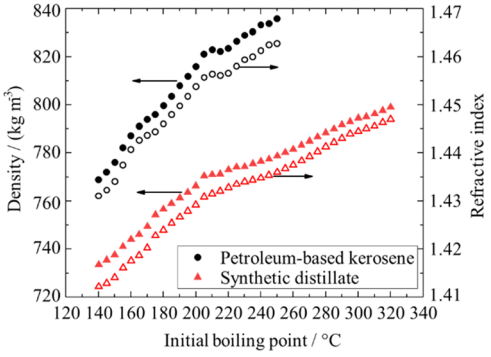

Figure 4. Density at 20 °C (filled symbols) and refractive index at 20 °C (nonfilled symbols) as a function of the initial boiling point for petroleum-based kerosene (circle) and the synthetic distillate (triangle). The final boiling point for all distillation cuts is 5 °C above the initial boiling point. The data is repeated from Tables 1, 2, S5, and S6, for visualization.

4.4. Solid−Liquid Phase Change Behavior. The solid−liquid phase change behavior was investigated using two techniques, via DSC and via optical determination. From the recorded DSC curves, two characteristic temperatures, the onset

https://doi.org/10.1021/acs.energyfuels.2c02625
Energy Fuels 2022, 36, 12563−12579

of freezing and the end of the melting endotherm, were obtained (see Figure 1).

4.4.1. Temperature of Phase Transition. When comparing the results obtained from optical determination with the characteristic temperatures from DSC analysis (see Figure 5 and Table 6), the end of the melting endotherm is equal to the optically determined freezing point within the reproducibility of the optical determination (±1.3 °C).

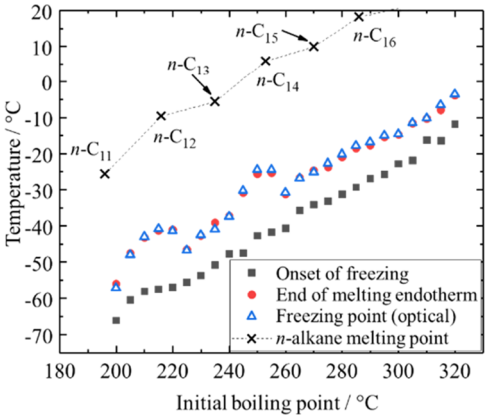

Figure 5. Onset of freezing and end of the melting endotherm in DSC analyses (filled symbols) and the optically determined freezing point (nonfilled symbols) of the synthetic distillate cuts as a function of their initial boiling point. The final boiling point is 5 °C above the initial boiling point. The data is repeated from Table 6 for visualization. Literature-reported[52] melting points of n-alkanes are shown for reference.

The optically determined freezing represents the freezing point determined via ASTM D2386 because it was calibrated using samples characterized via ASTM D2386 and the analysis method is similar to that described in ASTM D2386.[19] As the temperature at the end of the melting endotherm determined via DSC is equivalent to the optically determined freezing point for all analyzed distillation cuts, it can be concluded that the ASTM D2386 freezing point of such materials can be equally determined via DSC analysis.

A similar observation has been made in the literature for the determination of the freezing point of (wide-boiling) jet and diesel fuels and model hydrocarbon mixtures.[45,46] This is confirmed in our work by the good agreement between the ASTM D2386 freezing point and the end of the melting endotherm during DSC analysis.

The end of the melting endotherm was not affected significantly by the heating rate. This was tested only for *n*-decane and the synthetic distillate cut with a boiling range of 230−235 °C. The end of the melting endotherm was within ±0.5 °C for both samples at heating rates of 2 and 10 °C min^{-1}, respectively. This is in line with literature observations.[45,47]

The onset of freezing for any sample as extracted from the DSC curves is significantly lower than the end of the melting endotherm (Figure 1). The temperature difference (supercooling) ranges between 6.0 and 18.2 °C, respectively (see Tables 5 and 6). A similar degree of supercooling has been observed in the literature for the analysis of wide-boiling fuels.[45] Both the synthetic distillate and the petroleum-based kerosene exhibited supercooling. Kinetic effects related to nucleation have been linked to a shift in the onset of freezing with a change in the cooling rate of the DSC analysis.[47,48] In this study, only the 230−235 °C cut of the synthetic distillate was analyzed using two different cooling rates, namely, −2 and −10 °C min^{-1}. The higher cooling rate led to a decrease in the measured onset of freezing by 4 °C.

Of practical significance is that the onset of freezing did not correlate with the ASTM D2386 freezing point and that it changed with experimental conditions. Therefore, the onset of freezing from DSC analysis should not be used to draw conclusions about the ASTM D2386 freezing point, and only the end of the melting endotherm from DSC analysis can be used for this purpose.

4.4.2. Enthalpy of Phase Change versus Boiling Point. Generally, both the petroleum-based kerosene and the synthetic distillate exhibit an increasing trend of the onset of freezing, end of the melting endotherm, and the optically determined freezing point with increasing boiling point (see Tables 5 and 6). Also, there is a tendency for an increase in the phase change enthalpy with boiling point.

There are two parts to this observation. The first part has to do with the amount of material that participates in the phase change. The molar mass increases with increasing boiling point and therefore the amount of material that crystallizes at −70 °C is likely to increase for higher boiling fractions. Hence, the enthalpy of the phase change does not represent the enthalpy of freezing of the whole sample but the enthalpy of crystallization of a fraction of the sample that solidified during when cooling to −70 °C. A lower value for the enthalpy of phase change during freezing than the enthalpy of phase change during melting would indicate that freezing was incomplete during dynamic cooling and that additional freezing took place during the isothermal period at −70 °C. Further supercooling to lower temperatures might lead to a higher fraction of the sample crystallizing; therefore, the data does not represent a heat of fusion as defined for a pure material.

The second part has to do with the enthalpy of phase change of the material involved in the phase change. The enthalpy of phase change is related to the entropy change; it is sensitive to structure, which is a topic discussed extensively by Bondi.[49] It has been suggested that the amount of crystallized paraffins can be calculated from the phase change enthalpies in lubrication oils[50] and diesel fuels.[51] Given the low repeatability of the analysis for the kerosene cuts (±2 J g^{-1}), such analysis is not carried out in the present work. The increased phase change enthalpy with boiling point of the cut is left as an empirical observation.

4.4.3. Temperature of Phase Change versus Boiling Point. The onset of freezing increases with the boiling point for both materials. However, for the synthetic distillate, there are two distinct boiling ranges in which the progression of the end of the melting endotherm (or the optically determined freezing point) versus the boiling point exhibits local maxima (see Figure 5). The cut with an initial boiling point of 205 °C exhibits the same end of the melting endotherm as the cut with the initial boiling point 225 °C, and the cuts between these indicated cuts exhibit a higher end of melting isotherms (see Figure 5). This behavior repeats in the boiling range of 240−265 °C. A similar behavior in the boiling range of 205−225 °C was observed also for the petroleum-based kerosene material (see Table 5).

It has been stated that the melting point (equal to ASTM D2386 freezing point or the end of the DSC melting endotherm) of jet fuels is determined by the highest boiling *n*-alkane present in significant concentrations (above about 0.5 wt %).[45,52] The melting point versus boiling point plot of

https://doi.org/10.1021/acs.energyfuels.2c02625
Energy Fuels 2022, 36, 12563−12579

n-alkanes shows a "zigzag" behavior (see Figure 5).[53] Uneven-numbered *n*-alkanes show a lower melting point than expected from interpolation between the melting points of even-numbered *n*-alkanes or vice versa. This has been explained by a less dense packing of uneven-numbered *n*-alkanes compared to even-numbered *n*-alkanes,[54] which lowers the volumetric expansion during melting and thus reduces the melting entropy and enthalpy.[49]

The local maxima at the end of the melting endotherm versus boiling point plot of the synthetic distillate shown in Figure 5 coincide with the boiling point of the even-numbered *n*-alkanes *n*-dodecane and *n*-tetradecane, which also show higher melting point temperatures than their uneven-numbered neighbors. This is an indication that a particularly high concentration of these molecules in the boiling ranges of 210−225 and 250−260 °C is responsible for the unexpectedly high melting points.

There is no such behavior around the boiling point of *n*-hexadecane. However, the sample was obtained from hydrocracking and it is known that the degree of isomerization increases with carbon number during hydrocracking.[55] Therefore, a lower mass fraction of *n*-alkanes is expected in the boiling range of *n*-hexadecane.

Due to the complexity associated with connecting the freezing temperature and the molecular structure, the local maxima of freezing points with increasing boiling point are left as an observation. Nevertheless, for blending of wide-cut fuels, which are mixtures of cuts such as the ones discussed in this paper, this observation is pertinent.

5. CONCLUSIONS

The goal of this study was to identify whether the viscosity−temperature dependency and the predicted low-temperature viscosity of synthesized paraffinic kerosenes and petroleum-derived kerosenes were comparable. For this purpose, the temperature-dependent properties of narrow cut distillation fractions of a synthetic distillate (from wax hydrocracking) and petroleum-based kerosene were experimentally determined over the measurement temperature range +60 to −60 °C. The following conclusions were drawn.

(a) The viscosity−temperature dependence of the synthesized paraffinic kerosenes and petroleum-derived kerosene narrow cuts was described by MacCoull's equation in ASTM D341 with comparable accuracy (relative deviation <5%).

(b) Using a combination of the present work and the literature, it was indicated that broadening or narrowing the distillation range of synthesized paraffinic kerosene did not affect adherence to the viscosity−temperature relationship described in ASTM D341.

(c) When the viscosity−temperature relationship in ASTM D341 is employed for the prediction of the kinematic viscosity at −40 °C by extrapolating data measured at ≥−20 °C, the maximum difference between estimated and measured viscosity at −40 °C was 6.6% in all cuts analyzed in this study. This difference is higher than the experimental reproducibility of the kinematic viscosity following ASTM D7042, which is 2.1%. In addition, extrapolation has a risk of bias. For heavier kerosene cuts (>200 °C boiling), the extrapolation underpredicts the −40 °C viscosity.

(d) For both synthetic and petroleum-derived narrow cuts, cut-to-cut changes in viscosity appear to be determined by the increase in average molar mass rather than compound class compositional changes.

(e) Good agreement was found between the end of the melting endotherm obtained by differential scanning calorimetry (DSC) and the freezing point determined according to ASTM D2386 within the reproducibility of the optical determination (±1.3 °C).

(f) The freezing point of narrow distillation cuts exhibits local maxima and minima when plotted against the boiling point of the distillation cuts. These changes appear to be related to the freezing point characteristics of the *n*-alkanes in the distillation cuts.

■ ASSOCIATED CONTENT

Supporting Information

The Supporting Information is available free of charge at https://pubs.acs.org/doi/10.1021/acs.energyfuels.2c02625.

Additional information on petroleum kerosene composition (Table S1); carbon number distribution of paraffin wax (Table S2); distillation mass balance of petroleum kerosene (Table S3); distillation mass balance of the hydrocracking product (Table S4); refractive index, calculated molar mass, and molar refractivity (Tables S5 and S6); Viscosity and density analysis - raw and additional data (Tables S7 and S8); parameter for the MacCoull equation determined from viscosity data at different temperature ranges (Tables S9 and S10); gas chromatogram of the petroleum-based kerosene (Figure S1); aromatic volume fraction (HPLC) of petroleum-based kerosene cuts (Figure S2); and experimental and predicted viscosity of selected synthetic distillate cuts (Figure S3) (PDF)

■ AUTHOR INFORMATION

Corresponding Author

Felix Link − *Department of Chemical and Materials Engineering, University of Alberta, Edmonton, Alberta T6G 1H9, Canada;* orcid.org/0000-0002-1254-3569; Email: flink@ualberta.ca

Author

Arno de Klerk − *Department of Chemical and Materials Engineering, University of Alberta, Edmonton, Alberta T6G 1H9, Canada;* orcid.org/0000-0002-8146-9024

Complete contact information is available at: https://pubs.acs.org/10.1021/acs.energyfuels.2c02625

Notes

The authors declare no competing financial interest.

■ ACKNOWLEDGMENTS

The experimental investigation was funded by the Natural Sciences and Engineering Research Council (NSERC) of Canada Discovery Grant program, with salary support from Greenfield Global and MITACS.

■ REFERENCES

(1) Organ, R. J. Discussion on Uses of the Specifications for Aviation Turbine Fuels (ASTM D1655) and Aviation Gasoline (ASTM D910). In *Fuel Specifications: What They Are, Why We Have Them, and How They Are Used*; Rand, S. J.; Verstuyft, A. W., Eds.; ASTM Manual Series:

MNL69; ASTM International: West Conshohocken, PA, 2016; pp 39−82.
(2) ASTM D1655-21. *Standard Specification for Aviation Turbine Fuel*; ASTM International: West Conshohocken, PA, 2021.
(3) Coordinating Research Council. *Handbook of Aviation Fuel Properties*, CRC Report 663, 2nd ed.; Coordinating Research Council: Alpharetta, GA, 2014, with 2016 revision.
(4) ASTM D7566-21. *Standard Specification for Aviation Turbine Fuel Containing Synthesized Hydrocarbons*; ASTM International: West Conshohocken, PA, 2021.
(5) ASTM D341-20e1. *Standard Practice for Viscosity−Temperature Equations and Charts for Liquid Petroleum or Hydrocarbon Products*; ASTM International: West Conshohocken, PA, 2020.
(6) Hadaller, O. J.; Johnson, J. M. *World Fuel Sampling Program*, CRC Report 647; Coordinating Research Council: Alpharetta, GA; 2006.
(7) Moses, C. A.; Roets, P. N. J. Properties, Characteristics, and Combustion Performance of Sasol Fully Synthetic Jet Fuel. *J. Eng. Gas Turbines Power* **2009**, *131*, No. 041502.
(8) Heyne, J.; Rauch, B.; Le Clercq, P.; Colket, M. Sustainable Aviation Fuel Prescreening Tools and Procedures. *Fuel* **2021**, *290*, No. 120004.
(9) ASTM D4054-22. *Standard Practice for Evaluation of New Aviation Turbine Fuels and Fuel Additives*; ASTM International: West Conshohocken, PA, 2020.
(10) Lamprecht, D. Fischer−Tropsch fuel for use by the U.S. military as battlefield-use fuel of the future. *Energy Fuels* **2007**, *21*, 1448−1453.
(11) Moses, C. A. *Comparison of Semi-Synthetic Jet Fuels—Final Report*, CRC Project No. AV-2-04a; YUMPU Publishing, 2008.
(12) Fortin, T. J.; Laesecke, A. Viscosity measurements of aviation turbine fuels. *Energy Fuels* **2015**, *29*, 5495−5506.
(13) ASTM D7169-20. *Standard Test Method for Boiling Point Distribution of Samples with Residues Such as Crude Oils and Atmospheric and Vacuum Residues by High Temperature Gas Chromatography*; ASTM International: West Conshohocken, PA, 2020.
(14) Link, F.; Halmenschlager, C. M.; Chauhan, G.; De Klerk, A. Wax Hydrocracking over Pt/SiO_2-Al_2O_3 at 2 MPa: Product Characterization and Its Implications for Catalysis. *Energy Fuels* **2021**, *35*, 5252−5263.
(15) Shepard, A. F.; Henne, A. L.; Midgley, T. Physical Properties of the Normal Paraffin Hydrocarbons, Pentane to Dodecane. *J. Am. Chem. Soc.* **1931**, *53*, 1948−1958.
(16) Mondieig, D.; Rajabalee, F.; Metivaud, V.; Oonk, H. A. J.; Cuevas-Diarte, M. A. N-Alkane Binary Molecular Alloys. *Chem. Mater.* **2004**, *16*, 786−798.
(17) ASTM D4052-18a. *Standard Test Method for Density, Relative Density, and API Gravity of Liquids by Digital Density Meter*; ASTM International: West Conshohocken, PA, 2018.
(18) ASTM D7042-21. *Standard Test Method for Dynamic Viscosity and Density of Liquids by Stabinger Viscometer (and the Calculation of Kinematic Viscosity)*; ASTM International: West Conshohocken, PA, 2021.
(19) ASTM D2386-19. *Standard Test Method for Freezing Point of Aviation Fuels*; ASTM International: West Conshohocken, PA, 2019.
(20) ASTM D6379-21. *Standard Test Method for Determination of Aromatic Hydrocarbon Types in Aviation Fuels and Petroleum Distillates*; ASTM International: West Conshohocken, PA, 2019.
(21) Altgelt, K. H.; Boduszynski, M. M. *Composition and Analysis of Heavy Petroleum Fractions*; CRC Press: Boca Raton, 1994; pp 159−199.
(22) Shi, Q.; Zhao, S.; Xu, Z.; Chung, K. H.; Zhang, Y.; Xu, C. Distribution of Acids and Neutral Nitrogen Compounds in a Chinese Crude Oil and Its Fractions: Characterized by Negative-Ion Electrospray Ionization Fourier Transform Ion Cyclotron Resonance Mass Spectrometry. *Energy Fuels* **2010**, *24*, 4005−4011.
(23) Mohammed, A.-H. A.-K.; Attiya, H. G.; Khudair, H. A. K. The Relationships between the Physical and Chemical Properties of Narrow Fractions Distilled From Mixed Kirkuk and Sharki-Baghdad Crude Oils. *Iraqi J. Chem. Pet. Eng.* **2008**, *9*, 1−8.
(24) Höhne, G. W. H.; Hemminger, W. F.; Flammersheim, H.-J. *Differential Scanning Calorimetry*, 2nd ed.; Springer: Heidelberg, 2003; pp 115−146.
(25) Bondi, A. Viscosity and Molecular Structure. In *Rheology*; Eirich, F. R., Ed.; Academic Press: New York, 1967; Vol. 4, pp 1−83.
(26) Edwards, T. *Reference Jet Fuels for Combustion Testing*, AIAA Report; Air Force Research Laboratory: Dayton, OH; 2017.
(27) Bucknell, R. L. *Influence of Fuels and Lubricants on Turbine Engine Design and Performance, Fuel and Lubricant Analyses*, AFAPL Report AD-769 309. Pratt and Whitney: West Palm Beach, FL; 1973.
(28) Kim, D.; Violi, A. Uncertainty-Based Weight Determination for Surrogate Optimization. *Combust. Flame* **2022**, *237*, No. 111850.
(29) Weisser, K. L.; Turgeon, R. T. *90/10 JP-5 Synthesized Iso-paraffin Specification and Fit-for-purpose Test Results*, NAVAIR report 441/14-010; NAVAIR—Naval Air Systems Command: Patuxent River, MD, 2014.
(30) Luning Prak, D. J.; Fries, J. M.; Gober, R. T.; Vozka, P.; Kilaz, G.; Johnson, T. R.; Graft, S. L.; Trulove, P. C.; Cowart, J. S. Densities, Viscosities, Speeds of Sound, Bulk Moduli, Surface Tensions, and Flash Points of Quaternary Mixtures of n-Dodecane (1), n-Butylcyclohexane (2), n-Butylbenzene (3), and 2,2,4,4,6,8,8-Heptamethylnonane (4) at 0.1 MPa as Potential Surrogate Mixtures for Military Jet Fuel, JP-5. *J. Chem. Eng. Data* **2019**, *64*, 1725−1745.
(31) Bruno, T. J.; Laesecke, A.; Outcalt, S. L.; Seelig, H.-D.; Smith, B. L. *Properties of a 50/50 Mixture of Jet-A + S-8 (NISTIR 6647)*; National Institute of Standards and Technology: Boulder, CO, 2007.
(32) Lamprecht, D. Fischer−Tropsch fuel for use by the U.S. military as battlefield-use fuel of the future. *Energy Fuels* **2007**, *21*, 1448−1453.
(33) Pires, A. P. P.; Han, Y.; Kramlich, J.; Garcia-Perez, M. Chemical Composition and Fuel Properties of Alternative Jet Fuels. *BioResources* **2018**, *13*, 2632−2657.
(34) Giller, E. B.; Drickamer, H. G. Viscosity of Normal Paraffins near the Freezing Point. *Ind. Eng. Chem.* **1949**, *41*, 2067−2069.
(35) Riazi, M. R. *Characterization and Properties of Petroleum Fractions*, ASTM Manual Series: MNL50; ASTM International: West Conshohocken, 2005; pp 30−151.
(36) Abbott, M. M.; Kaufmann, T. G.; Domash, L. A Correlation for Predicting Liquid Viscosities of Petroleum Fractions. *Can. J. Chem. Eng.* **1971**, *49*, 379−384.
(37) Poling, B. E.; Prausnitz, J. M.; O'Connell, J. P. *The Properties of Gases and Liquids*, 5th ed.; McGraw-Hill: New York, 2000.
(38) Knapstad, B.; Skjølsvlk, P. A.; Øye, H. A. Viscosity of Pure Hydrocarbons. *J. Chem. Eng. Data* **1989**, *34*, 37−43.
(39) Oswal, S. L.; Maisuria, M. M.; Gardas, R. L. Viscosity of Binary Mixtures of Cycloalkane with Cycloalkane, Alkane and Aromatic Hydrocarbon at 303.15 K. *J. Mol. Liq.* **2003**, *108*, 199−215.
(40) Wang, X.; Jia, T.; Pan, L.; Liu, Q.; Fang, Y.; Zou, J. J.; Zhang, X. Review on the Relationship Between Liquid Aerospace Fuel Composition and Their Physicochemical Properties. *Trans. Tianjin Univ.* **2021**, *27*, 87−109.
(41) Dutt, N. V. K.; Prasad, D. H. L. Atomic and Structural Contributions to Molar Refraction and Extension to Mixtures. *Phys. Chem. Liq.* **1996**, *33*, 171−179.
(42) Katz, D. L.; Firoozabadi, A. Predicting Phase Behavior of Condensate/Crude-Oil Systems Using Methane Interaction Coefficients. *J. Pet. Technol.* **1978**, *30*, 1649−1655.
(43) Muller, H.; Saleem, Q.; Alawi, E. A.; Alsewdan, D. A.; Naqvi, I. A. S.; Saleh, A. H.; Rowaished, T. A. Narrow Distillation Cuts for an Improved Characterisation of Crude Oil: An Insight on Heteroatoms in Heavy Fraction Molecules. *Int. J. Oil, Gas Coal Technol.* **2021**, *26*, 40−59.
(44) De Klerk, A. *Fischer−Tropsch Refining*; Wiley-VCH: Weinheim, 2011; p 277.
(45) Moynihan, C. T.; Shahriari, M. R.; Bardakci, T. Thermal Analysis of Melting and Freezing of Jet- and Diesel Fuels. *Thermochim. Acta* **1982**, *52*, 131−141.
(46) Oakley, J. H.; Hughes, T. J.; Graham, B. F.; Marsh, K. N.; May, E. F. Determination of Melting Temperatures in Hydrocarbon Mixtures

by Differential Scanning Calorimetry. *J. Chem. Thermodyn.* **2017**, *108*, 59−70.
(47) Hammami, A.; Mehrotra, A. K. Non-Isothermal Crystallization Kinetics of Binary Mixtures of n-Alkanes: Ideal Eutectic and Isomorphous Systems. *Fuel* **1996**, *75*, 500−508.
(48) Widmor, N.; Ervin, J. S.; Zabarnick, S.; Vangness, M. Studies of Jet Fuel Freezing by Differential Scanning Calorimetry and Cold-Stage Microscopy. *J. Eng. Gas Turbines Power* **2003**, *125*, 34−39.
(49) Bondi, A. *Physical Properties of Molecular Crystals, Liquids, and Glasses*; John Wiley & Sons: New York, 1968.
(50) Noel, F. Thermal Analysis of Lubricating Oils. *Thermochim. Acta* **1972**, *4*, 377−392.
(51) Claudy, P.; Létoffé, J. M.; Neff, B.; Damin, B. Diesel Fuels: Determination of Onset Crystallization Temperature, Pour Point and Filter Plugging Point by Differential Scanning Calorimetry. Correlation with Standard Test Methods. *Fuel* **1986**, *65*, 861−864.
(52) Solash, J.; Hazlett, R. N.; Hall, J. M.; Nowack, C. J. Relation between Fuel Properties and Chemical Composition. 1. Jet Fuels from Coal, Oil Shale and Tar Sands. *Fuel* **1978**, *57*, 521−528.
(53) Streiff, A. J.; Hulme, A. R.; Cowie, P. A.; Krouskop, N. C.; Rossini, F. D. Purification, Purity, and Freezing Points of Sixty-Four American Petroleum Institute Standard and Research Hydrocarbons. *Anal. Chem.* **1955**, *27*, 411−415.
(54) Boese, R.; Weiss, H.-C.; Bläser, D. The Melting Point Alternation in the Short-Chain n-Alkanes: Single-Crystal X-Ray Analyses of Propane at 30 K and of *n*-Butane to *n*-Nonane at 90 K. *Angew. Chem., Int. Ed* **1999**, *38*, 988−992.
(55) Weitkamp, J.The Influence of Chain Length in Hydrocracking and Hydroisomerization of *n*-Alkanes. In *Hydrocracking and Hydrotreating*; Ward, J. W.; Qader, S. A., Eds.; ACS Symposium Series; American Chemical Society: Washington, DC, 1975; Vol. *20*, pp 1−27.

https://doi.org/10.1021/acs.energyfuels.2c02625
Energy Fuels 2022, 36, 12563−12579